Journal of Materials Science: Materials in Electronics (2019) 30:9045–9050
https://doi.org/10.1007/s10854-019-01236-w

Solution blow spinning control of morphology and production rate of complex superconducting $YBa_2Cu_3O_{7-x}$ nanowires

M. Rotta[1,2] · M. Motta[3] · A. L. Pessoa[1] · C. L. Carvalho[1] · W. A. Ortiz[3] · R. Zadorosny[1]

Received: 14 December 2018 / Accepted: 27 March 2019 / Published online: 3 April 2019

Abstract
Nanostructured materials have the potential to be applied in different areas ranging from electronics to medicine. Techniques for preparation of nanomaterials with a high production rate are essential to make them commercially available. In this work, complex superconducting $YBa_2Cu_3O_{7-x}$ wires were prepared by using the solution blow spinning technique with different solution injection rates (SIRs): 60, 80 and 100 µL/min. We show that the diameter of the YBCO wires increases from 258 to 954 nm for higher SIRs without any trace of secondary phases as investigated by X-ray diffractograms. Nonetheless, SIR does not supply the real ceramic production rate, which is 4.7 to 33 times higher than the rates of equivalent ceramics produced by Electrospinning. Furthermore, the magnetic properties of the YBCO wires were verified, presenting similar superconducting responses.

1 Introduction

The remarkable properties of materials at the nanoscale have placed them into the focus of basic and applied research [1–3]. To obtain nanomaterials, versatile and controllable techniques have been developed to tailor the intended properties of the specimens, as well as enhance their production rate [3, 4]. Non-woven micro- and nanofibers have attracted a lot of attention since they can be applied as optical sensors and piezoelectric devices [5–7], once their sensitivity increases due to the larger surface area per unit mass. Among several methods to produce fibers [8], electrospinning (ES) [9–13] and solution blow spinning (SBS) [11, 14–18] have recently gained prominence due to their simplicity and low cost. To produce ceramic fibers, ES and SBS can be combined with sol–gel processing to prepare nanowires for a variety of materials, such as $BaTiO_3$ [19–21], TiO_2 [15], ZnO [22], Mullite [23], and YBCO [18, 24].

The ES process has been known and used for more than a century [25] and has presented disadvantages such as a low production rate, requiring the application of high voltages, and the use of solutions with high dielectric constants [14]. Alternatively, SBS is less expensive and does not require either solutions with high dielectric constants or a conducting collector. Additionally, its production rate for the final ceramic material can be higher than that of ES, making SBS a promising candidate for supplying an increased demand for nanofibers.

For both SBS and ES, the ratio between metallic salts (MS) and the amount of polymer (PM) is of great importance in the production and morphology of ceramic materials [14]. However, several papers [11, 17, 18, 24] have not considered the ceramic production rate (CPR), reporting only the solution injection rate (SIR), which is a polymeric fiber productivity metric. Nevertheless, as the same amount of precursor solution can have different MS:PM ratios (lower or higher quantities of metallic ions), the use of SIR as a measurement could create confusion about the productivity of ceramic. Thus, the adoption of CPR as a production metric would lead to more consistent and reliable production rate measurement, since it represents the production rate of the final ceramic fiber.

Regarding the production of YBCO nanowires, one of the most important issues is the preparation of samples which

✉ R. Zadorosny
rafael.zadorosny@unesp.br

[1] Faculdade de Engenharia de Ilha Solteira, Universidade Estadual Paulista (UNESP), Av. Brasil 56, Centro, Ilha Solteira, SP 15.385-000, Brazil

[2] Instituto Federal de Educação, Ciência e Tecnologia de Mato Grosso do Sul (IFMS), Campus Três Lagoas, Rua Ângelo Melão, 790, Jardim das Paineiras, Três Lagoas, MS 79641-162, Brazil

[3] Departamento de Física, Universidade Federal de São Carlos, UFSCar, São Carlos, SP, Brazil

are as small and homogeneous as possible, although large enough to admit and maintain the superconducting state [25–27]. The threshold sizes for this are typically on the order of the superconducting penetration depth which, for YBCO, are around 100 nm [28]. The control of the diameter of superconducting nanowires and their geometry can guide us to new achievements related to their electrical and magnetic properties. Besides that, a superconducting nanowire can also be used as a sensor to detect single photons [29]. Thus, in this work superconducting ceramic nanowires of $YBa_2Cu_3O_{7-x}$ were produced by SBS. We prepared samples of the precursor solution with two different values of SIR and, consequently, CPR. The crystalline structure and morphology of the samples were studied by X-ray diffraction (XRD) and scanning electron microscopy (SEM). Temperature-dependent magnetization curves were obtained in order to investigate the superconducting properties of the final specimens. Furthermore, parameters such as concentration of polymer and acetates, SIR, and CPR, are compared with data reported in other studies in literature using SBS and ES.

2 Experimental procedures

In order to produce the precursor solution to be blown, stoichiometric amounts of acetates (Ac) of Y, Ba, and Cu were weighed in a molar ratio of 1:2:3. The amount of polyvinyl pyrrolidone (PVP) (MW 360,000 g/mol) was calculated based on a Ac:PVP weight ratio of 5:1. The final polymer solution was chosen to have a 5 wt% PVP concentration since in a previous analysis, such concentration resulted in a solution whose viscosity generated continuous jets and bead free fibrous samples. The acetates and PVP were dissolved in a solution of 14% propionic acid, 21% acetic acid, and 65% methanol [24].

Using the SBS technique, the precursor solution described previously was injected in an inner needle with three different values of SIR: (1) 60 µL/min (sample S6) (2) 80 µL/min (sample S8) and (3) 100 µL/min (sample S10). The emerging jet was blown on a collector at a working distance of 40 cm with an angular velocity of 40 rpm by pressurized air released in an outer needle. In order to keep the polymer solution jet uniform (without interruptions and droplets), the airflow pressure was set to (66 ± 12) kPa, (66 ± 12) kPa, and (50 ± 12) kPa for samples S6, S8 and S10, respectively. It is important to emphasize that the main parameters that affect the morphology of the nanofibers produced by SBS are SIR, airflow pressure, working distance, and the viscosity of the solution. During this process the working distance was constant, the viscosities were equal, and the air flow pressure was consistent; the only adjustable parameter used to control the diameters of the nanofibers was the SIR [15, 30].

The collected fibers in the green state were dried overnight at 100 °C and then heat-treated in two steps. In the first one, the samples were calcined at 450 °C for 3 h in an electric oven to eliminate organic material. Both heating and cooling were performed at 1 °C/min. In the second step, the samples were sintered in a tube furnace at 820 °C for 14 h and then at 925 °C for 1 h. After that, the samples were cooled down to 725 °C for 3 h and then to 450 °C for 12 h. The second step was entirely performed under oxygen flux. The heating rates from room temperature to 820 °C and from 820 to 925 °C were of 3 °C/min and 1 °C/min, respectively. The cooling rate from 925 to 750 °C was at 1 °C/min, and from 750 °C to room temperature (remaining 12 h at 450 °C) was 3 °C/min [24].

The influence of SIR on the microstructure of the samples was determined by using an EVO LS15 Zeiss SEM operated at 20 kV. XRD diffractograms were obtained in a Shimadzu XDR-6000 diffractometer with CuKα radiation. Measurements of the magnetization as a function of temperature were performed in a Quantum Design SQUID magnetometer MPMS-5S. The final ceramic fibers were measured under three different protocols: (1) Zero-Field Cooling (ZFC): the sample was cooled in a zero magnetic field (H = 0) to the lowest temperature before H was applied, (2) Field-Cooled Cooling (FCC): the sample was cooled to the superconducting critical temperature (T_c) under an applied magnetic field, and (3) Thermoremanence (TRM): the specimen was cooled to the lowest temperature under H before then the magnetic field was set to zero and the measurement was done on warming.

3 Results and discussion

Successful nanowire production using SBS is directly related to the synthesis of a precursor solution that provides high MS solubility in the polymer, resulting in a solution free of precipitates. The choice of acetates, the high solubility and volatility of the solvents, and the adoption of the PVP are of crucial importance. The PVP acts as a stabilizer, as its hydroxyl (–OH) limits metallic nanostructure production [31]. Its high solubility enables the use of a high rate of 5:1 for Ac:PVP; this resulted in CPRs of 6.2 mg/min, 8.2 mg/min, and 10.3 mg/min for samples S6, S8, and S10, respectively (Table 1). By comparison, the ES approach yields CPR values which are roughly 3% of those obtained via SBS, meaning that SBS can generate a substantially higher production of ceramic nanowires.

Representative SEM micrographs and diameter distributions of the produced polymer fibers (green state), as well as of the final ceramics, are shown in Fig. 1. Panels (a), (c) and (e) present the usual morphology: cylindrical shape and smooth surface with no beads along the green fibers.

Table 1 Comparison of the solution injection rate (SIR), the ceramic production rate (CPR), and the diameter of the YBCO wire for the produced samples and data published in other studies

Sample	Ratio [Ac:PVP]	SIR (μL/min)	CPR (mg/min)	YBCO wire diameter range (nm)
S6	5:1	60	6.2	206–310
S8	5:1	80	8.2	200–1300
S10	5:1	100	10.3	780–1188
Duarte et al. [17]	5:1	13.3	1.4	240–550
Duarte et al. [17]	1:1	13.3	0.3	120–300
Shen et al. [28]	1:1.6	50	2.2	110–150*

*This range refers to the external diameter of YBCO nanotubes with a wall thickness of 30–40 nm

Statistical analysis of fiber diameters returned an average value of (476 ± 92) nm for S6 (panel b), (611 ± 191) nm for S8 (panel d) and (1222 ± 242) nm for S10 (panel f). This demonstrates, in the range of the covered by this work, that the average fiber diameter in the green state increases as the injection rate rises.

The green samples were heat-treated at 450 °C to burn out the polymer PVP in a slow heating ramp rate to keep its cylindrical geometry arranged in a 3D network. Figure 1i–k show the morphology of the samples S6, S8 and S10, respectively, after the heat treatments described above. The images demonstrate that the wires are randomly oriented and present a rough appearance due to their multigrain structure. It means that there is a directional coalescence of neighboring grains with diffusion of atoms through neck formation, which is one of the stages of sintering. It has been also observed in powder YBCO samples prepared by the Pechini Method [32]. Furthermore, the average diameter values for the samples S6, S8, and S10 are (258 ± 52) nm (panel h), (562 ± 237) nm (panel j), and (984 ± 204) nm (panel l), respectively.

The evolution of the average diameter against the solution injection rate for the green and ceramic samples is summarized in Fig. 2. It can be noted that the average diameter of both sets of samples—green and ceramic—increases with increasing SIR. Besides that, the ceramic samples present a smaller diameter as compared to the green ones due to the elimination of the organic material.

The final column in Table 1 compares the diameters of S6, S8, and S10 with specimens prepared by ES. The diameter for S6 is similar to the sample obtained by Duarte et al. [18] with the same Ac:PVP ratio, although the production rate is 4.5 times larger. By using lower Ac:PVP ratios, Duarte et al. [18] and Shen et al. [33] created nanowires with smaller diameters as compared to our samples; however, the CPRs were also lower. It is important to point out that the samples prepared in reference 33 are YBCO nanotubes with wall thicknesses of 30–40 nm, which is a different morphology compared to our samples. As our focus here is to show the diameter control by the SIR and introduce the CPR parameter, henceforward, we will focus our analysis on the extreme SIR samples, i.e., on S6 and S10 ones.

After all heat treatments and morphologic characterizations were completed, the presence of the YBaCuO superconducting phase, and also some secondary phases, was verified by XRD measurements. Figure 3 shows similar results for both samples, with no trace of spurious phases and consistent with the *JCPDS-78-2269* card. Using the Debye–Scherrer equation, crystallite sizes were estimated to be (20.7 ± 1.7) nm for S6 and (22.0 ± 1.4) nm for S10.

Considering the XRD patterns, a superconducting transition had been expected for both samples. Figure 4 presents magnetization versus temperature curves for samples S6 (panel a) and S10 (panel b). The superconducting critical temperature was determined by taking the last measured point in the normal state while decreasing the temperature. The T_c values for S6 and S10 were 92.1 K and 93.1 K, respectively, similar to the value reported in references [31, 33].

In superconducting specimens, the ZFC protocol is a procedure tailored to evaluate the amount of flux excluded from the sample, whereas the FCC is capable of sensing how much flux is expelled from the specimen. The difference between the ZFC and FCC curves is associated with the flux trapped in the material defects. Figure 4a and b shows that there is more magnetic flux trapped in S10 than in S6; such behavior can be associated with a higher density of defects in the multigrain wires. Consistently, TRM curves confirm such behavior since they are a direct measurement of the flux trapped inside the samples.

4 Conclusion

SBS is a versatile and efficient technique for preparing complex ceramic wires. The average diameters of the YBCO fibers reached 258 nm, 562 nm and 984 nm with solution injection rates of 60 μL/min, 80 μL/min and 100 μL/min respectively, since small diameters increase the surface area, it was showed that SIR is an important

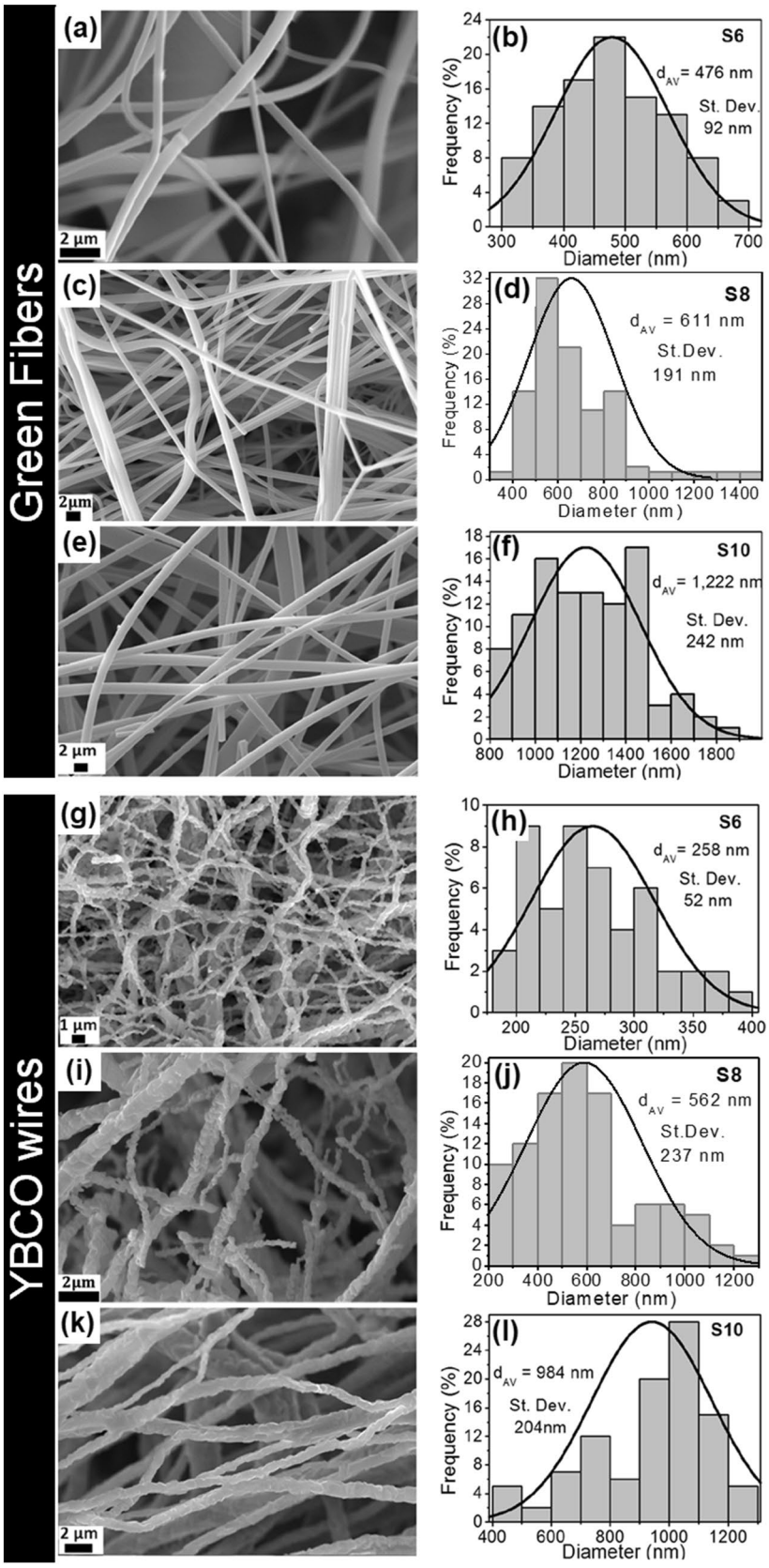

Fig. 1 SEM micrograph of green samples S6 (**a**), S8 (**c**) and S10 (**e**) and their diameter distribution with average values of (476 ± 92) nm (**b**), 611 ± 191 nm (**d**) and (1222 ± 242) nm (**f**), respectively. The SEM images of the fired fibers S6, S8 and S10 and their diameter distributions are shown in panels (**g**) through (**l**). The average diameter values were (258 ± 52) nm for S6 (**h**), (562 ± 237) nm for S8 (**j**) and (984 ± 204) nm for S10 (**l**)

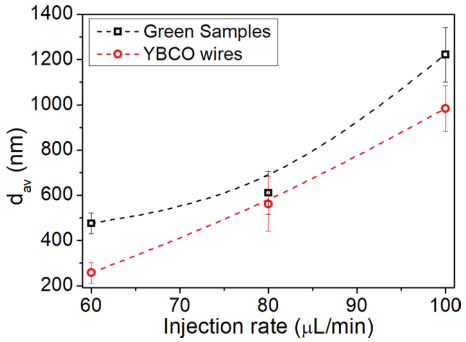

Fig. 2 Average diameter as a function of Injection rate for the green (squares) and ceramic (circles) samples. The dashed lines are guide for the eyes

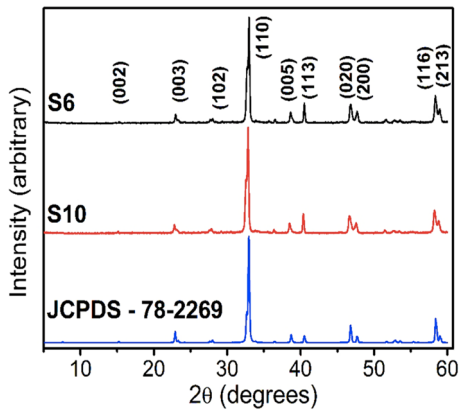

Fig. 3 XRD diffractograms taken at a scan rate of 0.02° (/min for samples S6 and S10, which are consistent with the *JCPDS-78-2269* reference card

parameter to obtain samples with the desirable sizes. Although SIR is the common parameter used to monitor the morphology of the fibers, the ceramic production rate is the most appropriate metric for such processes since it represents a reliable measurement of the real ceramic productivity. In our case, the CPR was 6.2 mg/min, 8.2 mg/min, and 10.3 mg/min for samples S6, S8, and S10, respectively, reaching values around 30 times greater than similar samples produced by the ES technique. Therefore, we suggest the term Ceramic Production Rate to refer to the production rate of ceramic structures by means of Spinning techniques.

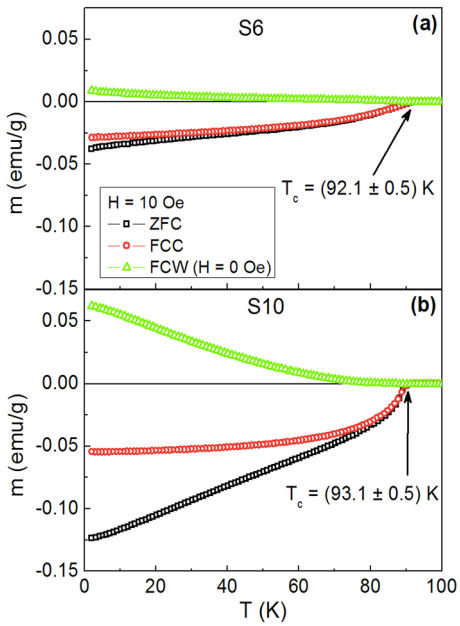

Fig. 4 Measurements of the magnetization as a function of temperature following the procedures ZFC, FCC, and TRM (see the main text) for samples S6 (**a**) and S10 (**b**), taken under an applied field H = 10 Oe with T_c of 92.1 K and 93.1 K, respectively

Acknowledgements We acknowledge the Brazilian agencies São Paulo Research Foundation (FAPESP, Grant 2016/12390-6), Coordenação de Aperfeiçoamento de Pessoal de Nível Superior - Brasil (CAPES) - Finance Code 001, National Council of Scientific and Technological Development (CNPq, grant 302564/2018-7) and Instituto Federal do Mato Grosso do Sul (IFMS).

References

1. Y. Xia, P. Yang, Y. Sun, Y. Wu, B. Mayers, B. Gates, Y. Yin, F. Kim, H. Yan, One-dimensional nanostructures: synthesis, characterization, and applications. Adv. Mater. **15**, 353–389 (2003)
2. S. Chaturvedi, N.D. Dave, Design process for nanomaterials. J. Mater. Sci. **48**, 3605–3622 (2013)
3. F. Piccinno, F. Gottschalk, S. Seeger, B. Nowack, Industrial production quantities and uses of ten engineered nanomaterials in Europe and the world. J. Nanopart. Res. **14**, 1109 (2012)
4. Q. Zhang, J.Q. Huang, W.Z. Quian, Y.Y. Zhang, F. Wei, The road for nanomaterials industry: a review of carbon nanotube production, post-treatment, and bulk applications for composites and energy storage. Small **9**, 1237–1265 (2013)
5. X.Y. Wang, S.H. Lee, C. Drew, K.J. Senecal, J. Kumar, L.A. Samuelson, Highly sensitive optical sensors using electrospun polymeric nanofibrous membranes. Mater. Res. Soc. Symp. Proc. **708**, 397–402 (2002)

6. X.Y. Wang, C. Drew, S.H. Lee, K.J. Senecal, J. Kumar, L.A. Samuelson, Electrospun nanofibrous membranes for highly sensitive optical sensors. Nano Lett. **2**, 1273–1275 (2002)
7. A.G. Scopelianos, US patent 5522879, 1996
8. A. Barhoum, M. Bechelany, A.S. Hamdymakhlouf (eds.), *Handbook of Nanofibers. Vol. I: Fundamental Aspects and Experimental Setup* (Springer, Berlin, 2018). ISBN: 9783319536545
9. N. Bhardwaj, S.C. Kundu, Electrospinning: a fascinating fiber fabrication technique. Biotechnol. Adv. India **28**, 325–347 (2010)
10. X.L. Zeng, M.R. Koblisschka, T. Karwoth, T. Hauet, U. Hartmann, Preparation of granular Bi-2212 nanowires by electrospinning. Supercond. Sci. Technol. **30**, 035014 (2017)
11. X.M. Cui, W.S. Lyoo, W.K. Son, D.H. Park, J.H. Choy, T.S. Lee, W.H. Park, Fabrication of $YBa_2Cu_3O_{7-\delta}$ superconducting nanofibres by electrospinning. Supercond. Sci. Technol. **19**, 1264–1268 (2006)
12. Z.M. Huang, Z.Y. Zhang, M. Kotaki, S. Ramakrishna, Compos. Sci. Technol. **63**, 2223 (2003)
13. C. Mu, Y. Song, A. Liu, X. Wang, J. Hu, H. Ji, H. Zhang, Electrospun Cu_2ZnSnS_4 microfibers with strong (112) preferred orientation: fabrication and characterization Chunhong. RSC Adv. **5**, 15749–15755 (2015)
14. E.S. Medeiros, G.M. Glenn, A.P. Klamczynski, W.J. Oorts, L.H.C. Mattoso, Solution blow spinning: a new method to produce micro- and nanofibers from polymer solutions. J. Appl. Polym. Sci. **113**, 2322–2330 (2009)
15. J.L. Daristotle, A.M. Behrens, A.D. Sandler, P. Kofinas, A review of the fundamental principles and applications of solution blow spinning. Appl. Mater. Interfaces **8**, 34951–34963 (2016)
16. J.E. Oliveira, E.A. Moraes, R.G.F. Costa, A.S. Afonso, L.H.C. Mattoso, W.J. Orts, E.S. Medeiros, Nano and submicrometric fibers of Poly(D, L-Lactide) obtained by solution Blow spinning: process and solution variables. J. Appl. Polym. Sci. **122**, 3396–3405 (2011)
17. E.A. Duarte, P.A. Quintero, M.W. Meisel, J.C. Nino, Electrospinning synthesis of superconducting BSCCO nanowires. Phys. C Supercond. Appl. **495**, 109–113 (2013)
18. E.A. Duarte, N.G. Rudawski, P.A. Quintero, M.W. Meisel, J.C. Nino, Electrospinning of superconducting YBCO nanowires. Supercond. Sci. Technol. **28**, 15006 (2015)
19. J. Yuh, J.C. Nino, W.A. Sigmund, Synthesis of barium titanate ($BaTiO_3$) nanofibers via electrospinning. Mater. Lett. **59**, 3645–3647 (2005)
20. J. Yuh, L. Perez, W.M. Sigmund, J.C. Nino, Sol–gel based synthesis of complex oxide nanofibers. J. Sol Gel Sci. Technol. **42**, 323–329 (2007)
21. J. Yuh, L. Perez, W.M. Sigmund, J.C. Nino, Electrospinning of complex oxide nanofibers. Physica E **37**, 254–259 (2007)
22. D.L. Costa, R.S. Leite, G.A. Neves, L.N.D.L. Santana, E.S. Medeiros, R.R. Menezes, Synthesis of TiO_2 and ZnO nano and submicrometric fibers by solution blow spinning. Mater. Lett. **183**, 109–113 (2016)
23. R.M.C. Farias, R.R. Menezes, J.E. Oliveira, E.S. Medeiros, Production of submicrometric fibers of mullite by solution blow spinning (SBS). Mater. Lett. **149**, 47 (2015)
24. M. Rotta, L. Zadorosny, C.L. Carvalho, J.A. Malmonge, L.F. Malmonge, R. Zadorosny, YBCO ceramic nano fibers obtained by the new technique of solution blow spinning. Ceram. Int. **42**, 16230–16234 (2016)
25. K. Xu, J.R. Heath, Long, highly-ordered high-temperature superconductor nanowire arrays. Nano Lett. **8**(11), 3845–3849 (2008)
26. A. Bezryadin, C.N. Lau, M. Tinkham, Quantum suppression of superconductivity in ultrathin nanowires. Nature **404**, 971 (2000)
27. M. Zgirski, K.P. Riikonen, V. Touboltsev, K. Arutyunov, Size dependent breakdown of superconductivity in ultranarrow nanowires. Nano Lett. **5**, 6 (2005)
28. C.P. Poole Jr., H.A. Farach, R.J. Creswick, *Superconductivity* (Academic Press, San Diego, 1995)
29. I. Holzman, Y. Ivry, Superconducting nanowires for single-photon detection: progress, challenges, and opportunities. Adv. Quantum Technol. (2019). https://doi.org/10.1002/qute.201800058
30. L. Nicodemo, L. Nicolais, Viscosity of bead suspensions in polymeric solutions. J. Appl. Polym. Sci. **18**, 2809–2818 (1974)
31. Y. Xiong, I. Washio, J. Chen, H. Cai, Z.Y. Li, Y. Xia, Poly(vinyl pyrrolidone): a dual functional reductant and stabilizer for the facile synthesis of noble metal nanoplates in aqueous solutions. Langmuir **22**, 8563–8570 (2006)
32. M. Motta, C.V. Deimling, M.J. Saeki, P.N. Lisboa-Filho, Chelating agent effects in the synthesis of mesoscopic-size superconducting particles. J. Sol Gel Sci. Technol. **46**, 201 (2008)
33. Z. Shen, Y. Wang, W. Chen, L. Fei, K. Li, H.L.W. Chan, L. Bing, Electrospinning preparation and high-temperature superconductivity of $YBa_2Cu_3O_{7-x}$ nanotubes. J. Mater. Sci. **48**, 3985–3990 (2013)